Design and Control of Wireless Permanent-Magnet Brushless DC Motors

Hui Wang, *Member, IEEE*, K. T. Chau, *Fellow, IEEE*, Wei Liu, *Member, IEEE*,
Stefan M. Goetz, *Member, IEEE*

Abstract—Recently, wireless power transfer for electric motor technology has been studied, where the primary side can drive the motor without physical contact, so the load motor can be employed in isolated environments. This paper proposes a wireless permanent-magnet brushless DC (PM-BLDC) motor. Prominently, the secondary side does not involve any motor control chip, as the motor is fully controlled by the WPT controller at the primary side. The key is to employ three widely orthogonal channels with six LC tuning circuits at the secondary side, which can replace the motor controller to regulate the secondary inverter. Thus, the robustness of the motor side is ruggedized and highly improved by eliminating the most fragile component, i.e., the controlling microchip. Circuit simulations and an experimental prototype verify and demonstrate that the proposed three-phase PM-BLDC motor can be driven wirelessly with a single primary controller from 400 to 4000 rpm with 20 mm wireless power transfer distance, and the transmission efficiency can be as high as 80.2%.

Index Terms—Wireless power transfer, permanent-magnet brushless DC motor, secondary controller-less.

I. INTRODUCTION

WIRELESS power transfer (WPT) has obtained a lot of interest due to its importance as a convenient feature in hand-held [1] and internet-of-things devices, vehicles [2], unmanned aerial vehicles (UAV) [3], as well as medical devices [4] and implants [5], effectively solving the problems of wire abrasion, sparking hazards, inconvenience, and most importantly inaccessibility [6]. Furthermore, WPT is particularly suitable for powering electric devices in harsh, sealed, or explosion-protected environments [4], such as wireless lighting [7], wireless heating [8], and wireless motoring [9].

As wire limitation is avoided, wireless motors have unique advantages in several special applications [10]. The first potential application is robotic arms. As robotic arms move and rotate irregularly, power lines may be twisted and need costly guidance, especially if the robotic arm rotates in one direction continuously. Also, for the wired electric motor, the reliability of the electrical condition may be impaired due to random movements of the robotic arm [11]. Thus, by employing wireless motors, robotic arms will have greater freedom of movement. Besides, in underwater robots, water may enter the motors from the robot joints, as the frequent movement of joints will cause aging and wear of the line protection layer. Thus, wireless motors have superiority as these can be completely sealed and avoid leakage problems.

In addition, wireless motors have great potential in the piping network. Traditionally, the piping motor is charged from the outside power grid, which is deployed along with the piping network. Thus, complex and expensive maintenance is inevitably required [12]. However, when charging the motor from the energy-carrying electric vehicle via WPT technology [13], the whole system will be more reliable, safe, and easy to maintain.

Moreover, in transportation, WPT is a strong candidate to replace the wear-and-tear pantographs to charge high-speed railway's motors, which could effectively reduce railway construction and maintenance costs [14].

Sato et al. proposed the first wireless motor, which employed WPT to charge the in-wheel motor to avoid cable abrasion [15]. However, the motor controller at the secondary side is a fragile bottleneck, can fail, and needs maintenance. Moreover, the communication between the primary side and the remote side is based on Bluetooth. Hence, the milliseconds of communication latency and generally uncontrolled timings may cause a control delay [16].

To avoid these bottlenecks, different kinds of single-controller wireless motors have been studied, such as wireless DC motors [17], wireless shaded-pole induction motors (SPIMs) [18], and wireless switched reluctance (SR) motors [19]. Also, the wireless resolver has been proposed, which can transfer timely position signals to the primary controller for all wireless motors [20]. However, wireless DC motors suffer from fragile carbon brushes and the commutator, which cost efficiency and wear off, while wireless SR motor and wireless

H. Wang and Stefan M. Goetz are with the Department of Electrical and Computer Engineering, Duke University, Durham, NC 27708, USA (e-mail: hui.wang@duke.edu; stefan.goetz@duke.edu).

K. T. Chau is with the Department of Electrical and Electronic Engineering, The Hong Kong Polytechnic University, 999077, Hong Kong (e-mail: k.t.chau@polyu.edu.hk).

W. Liu are with the Department of Electrical and Electronic Engineering, The University of Hong Kong, Pokfulam, Hong Kong (e-mail: liuwei@eee.hku.hk).

SPIM falls short in torque density without the use of the latest rare-earth permanent magnets (PMs) and due to their low power factor associated with driving their excitation through the AC supply.

Therefore, to solve these problems, a wireless single-controller brushless PM motor is required. PM brushless DC (PM-BLDC) motors with trapezoidal back-EMF offer high power density, efficiency, and low manufacturing costs [21]; hence, they serve in a variety of consumer electronics and industrial applications [22]. However, it should be mentioned that—different from SR motor and SPIM—most PM-BLDC motors require three or more phases of AC power, which is very difficult to acquire without a remote controller. Although self-drive circuits for single-phase AC power and three-phase DC power are proposed in [18] and [23], respectively, self-drive circuit for three-phase AC power is absent in the literature.

This paper proposes the first wireless PM-BLDC motor, which has high torque density and high reliability by eliminating the motor controller at the secondary side. The key is to employ a self-driving circuit at the secondary side. Importantly, the concept does not limit major design aspects of the load motor so that it could readily drive most existing PM-BLDC motors at the secondary side. To verify the validity of the proposed sensorless control strategy, detailed theoretical analysis and experimental results are provided in this paper.

This paper is organized as follows: Section II analyzes the system configuration and basic control principle. Subsequently, Section III discusses the system design and optimization. Section IV will be devoted to analyzing the system control performance. Experiments underpin the feasibility in Section V. Finally, Section VI concludes the paper.
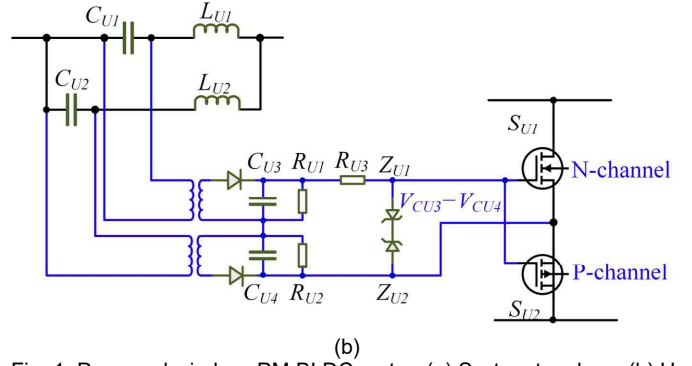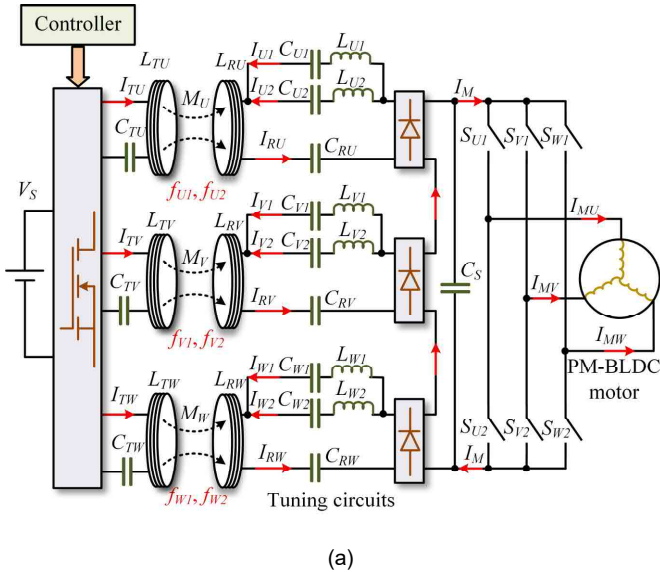

(a)

(b)

Fig. 1. Proposed wireless PM-BLDC motor. (a) System topology. (b) U-phase secondary self-drive circuit.

II. SYSTEM CONFIGURATION AND CONTROL PRINCIPLE

A. System Configuration

Fig. 1(a) depicts the topology of the proposed wireless PM-BLDC motor, where L_{TU}, C_{TU}, L_{RU}, C_{RU}, L_{TV}, C_{TV}, L_{RV}, C_{RV}, L_{TW}, C_{TW}, L_{RW}, and C_{RW} with subscripts U, V, and W denote three-phase WPT coils and corresponding compensation capacitors, respectively; I_{TU}, I_{TV}, I_{TW}, I_{RU}, I_{RV}, and I_{RW} are currents of three-phase transmitters and receivers with the same subscript, respectively; M_U, M_V, and M_W are mutual inductances between three-phase transmitters and receivers, respectively; L_{U1}, C_{U1}, L_{U2}, and C_{U2}, constitute U-phase two-channel LC tuning circuits, also L_{V1}, C_{V1}, L_{V2}, and C_{V2} constitute V-phase LC tuning circuits, while L_{W1}, C_{W1}, L_{W2}, and C_{W2} constitute W-phase LC tuning circuits, respectively; I_{U1}, I_{U2}, I_{V1}, I_{V2}, I_{W1}, and I_{W2} are the currents of the six-channel LC tuning circuits, respectively; C_S is the filtering and buffering capacitor after the bridge rectifier; S_{U1}, S_{U2}, S_{V1}, S_{V2}, S_{W1}, and S_{W2} form a secondary-side three-phase full-bridge inverter; I_{MU}, I_{MV} and I_{MW} are the three-phase motor currents, respectively, and I_M is total current of the motor; V_S denotes the input DC voltage of the primary side.

The primary side provides the three-phase high-frequency AC power for WPT, and the secondary side harvests this wireless power through the three-phase receiver. It should be mentioned that two frequencies are adopted for each phase of power transmission, while U-, V-, and W-phase transmitting and receiving sides are resonant at the middle frequencies with subscripts U, V, and W, respectively, which can be expressed as [24]

$$\begin{cases} \pi(f_{i1}+f_{i2})L_{Ti} = \dfrac{1}{\pi(f_{i1}+f_{i2})C_{Ti}} \\ \pi(f_{i1}+f_{i2})L_{Ri} = \dfrac{1}{\pi(f_{i1}+f_{i2})C_{Ri}} \end{cases} (i = U, V, W). \quad (1)$$

Also, six-channel LC tuning circuits are specially designed to resonate at the aforementioned six frequencies with the same subscript, which can be expressed as

$$\begin{cases} 2\pi f_{i1} L_{i1} = \dfrac{1}{2\pi f_{i1} C_{i1}} \\[3mm] 2\pi f_{i2} L_{i2} = \dfrac{1}{2\pi f_{i2} C_{i2}} \end{cases} \quad (i = U, V, W). \quad (2)$$

Further inspection of the system configuration in Fig. 1(a) indicates that there is no motor controller at the secondary side, as the voltages of capacitors in the LC tuning circuits serve for the actuation of the secondary inverter. Taking U-phase as an example, as shown in Fig. 1(b), the voltages of capacitors C_{U1} and C_{U2}, namely, V_{CU1} and V_{CU2}, are isolated, rectified, and stabilized through transformers, diodes, and capacitors. Hence, the acquired control signal $V_{CU3} - V_{CU4}$ can be used to control the N-channel and P-channel MOSFETs together. Two Zener diodes and one resistor limit the voltage between the gate and the source to protect the MOSFETs.

A wireless resolver provides the rotor position signal. As this part is proposed in the literature [25], and it is not the theme of this paper, this part is kept short in this paper.

To better illustrate the topology of the proposed wireless BLDC motors, key features, as well as the advantages and disadvantages, of some typical wireless motors and proposed systems are compared in Table I.

TABLE I
COMPARISON OF WIRELESS MOTORS

Types	Structural feature	Pros and cons
Dual-controller wireless motor [15]	• Cascaded WPT and conventional wired electric motors.	☑ All control methods are available. ☑ All electric motors (including PMSM) are available. ☒ The remote controller is fragile ☒ Control delay caused by Bluetooth communication interval
Wireless DC motor [17]	• The remote rectifier bridge rectifies the high-frequency energy and charges the DC motor directly.	☑ The size is very small. ☑ Easy to control. ☒ Only unidirectional movement. ☒ The brush needs regular maintenance.
Wireless SPIM [18]	• Two LC tuning circuits control the remote inverter.	☑ The size is very small. ☑ Easy to control. ☒ Only unidirectional movement. ☒ Low torque density.
Wireless SR motor [19]	• Each receiver and rectifier bridge charge one stator winding. • No remote inverter.	☑ Bidirectional movement. ☑ No active component at the remote side. ☒ Multi-receiver or multi-frequency WPT is needed. ☒ Low torque density.
Wireless BLDC motor	• Three pairs of WPT coils. • Six LC tuning circuits control a three-phase inverter.	☑ Bidirectional movement. ☑ High torque density. ☒ Multi-receiver and multi-frequency WPT is needed.

B. Motor Frequency Control

Depending on the position of the stator windings, the interior of the PM-BLDC motor can be divided into six sections, as shown in Fig. 2(a) [26]. For traditional wired PM-BLDC motors, the six-step commutation operation method is generally adopted, as shown in Fig. 2(b) and (c) [27]. To drive the PM-BLDC motor without the secondary controller, the primary side needs to charge two or three receivers for the 120° or 180° commutation method, respectively.

Taking the first sector in 120° commutation operation as an example, when the primary side charges the receiver U with frequency f_{U1} and receiver V with frequencies f_{V2}, simultaneously, only the first U-phase LC tuning circuit and second V-phase LC tuning circuit are resonant, as shown in Fig. 3(a). Thus, the currents I_{U1} and I_{V2} are basically equal to the receiver currents I_{RU} and I_{RV}, while the currents I_{U2} and I_{V1} are negligible because of missing resonance. Therefore, the voltages of C_{U1} and C_{V2}, namely V_{CU1} and V_{CV2}, are very high, while the voltages of C_{U2} and C_{V1}, namely, V_{CU2} and V_{CV1}, are very low. As a result, the control signal for U-phase $V_{CU3} - V_{CU4}$ is positive, and the control signal for V-phase $V_{CV3} - V_{CV4}$ is negative, while the control signal for the W-phase $V_{CW3} - V_{CW4}$ is zero. Thus, S_{U1} and S_{V2} are switched on, and the current flows in from the motor's U-phase winding and out from the V-phase winding.

Similarly, when the motor is running in the fifth sector with the 180° commutation operation method, as shown in Fig. 3(b), the primary side charges the receiver U, receiver V, and receiver W with frequencies f_{U2}, f_{V1}, and f_{W1}, respectively. Only the second U-phase LC tuning circuit, the first V-phase LC tuning circuit, and the first W-phase LC tuning circuit are resonant. Thus, the I_{U2}, I_{V1} and I_{W1} are basically equal to the receiver currents I_{RU}, I_{RV} and I_{RW}, while the currents I_{U1}, I_{V2} and I_{W2} are negligible because of non-resonance. Therefore, the voltages of C_{U2}, C_{V1} and C_{W1}, namely V_{CU2}, V_{CV1} and V_{CW1}, are very high, while the voltages of C_{U1}, C_{V2} and C_{W2}, namely, V_{CU1}, V_{CV2} and V_{CW2}, are very low. As a result, the control signal $V_{CU3} - V_{CU4}$ is negative, while $V_{CV3} - V_{CV4}$ and $V_{CW3} - V_{CW4}$ are positive. Thus, S_{U2}, S_{V1} and S_{W1} are switched on, and the current flows in from the motor's V-phase and W-phase winding and out from the U-phase winding.

Hence, energizing these three receivers sequentially can generate the desired control signals as shown in Fig. 4. Consequently, the PM-BLDC motor can rotate without involving the motor controller at the secondary side. Meanwhile, changing the phase sequence of the three-phase stator winding currents can readily change the direction of rotation.
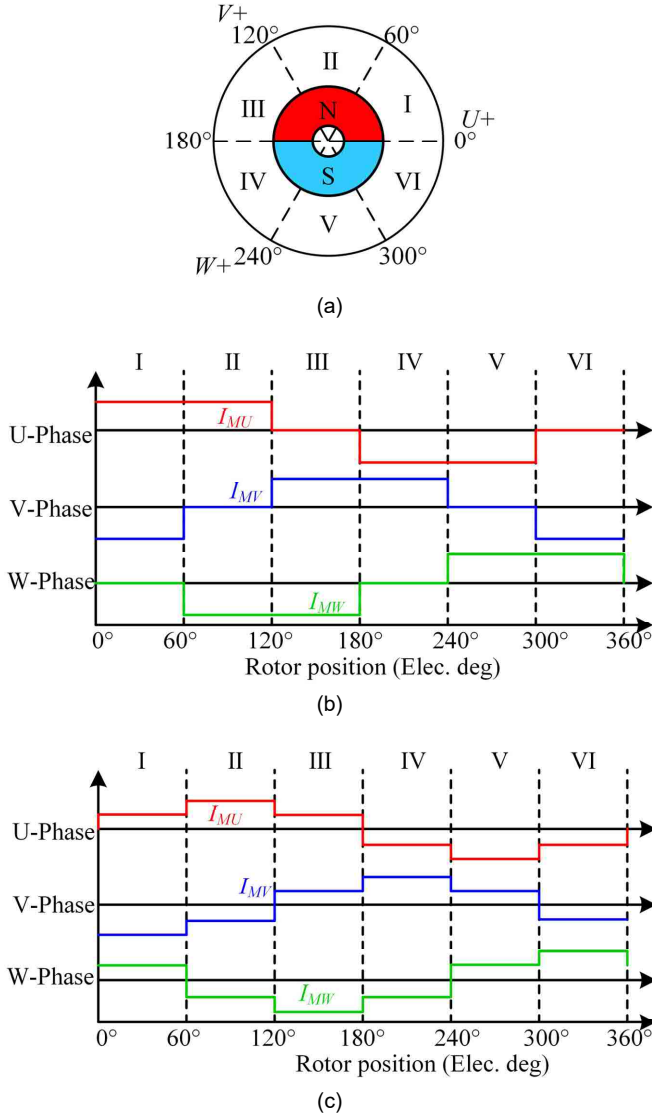
(a)

(b)

(c)

Fig. 2. Control of PM-BLDC motor. (a) Six sectors of PM-BLDC motor. (b) Motor currents under 120° commutation method. (c) Motor currents under 180° commutation method.
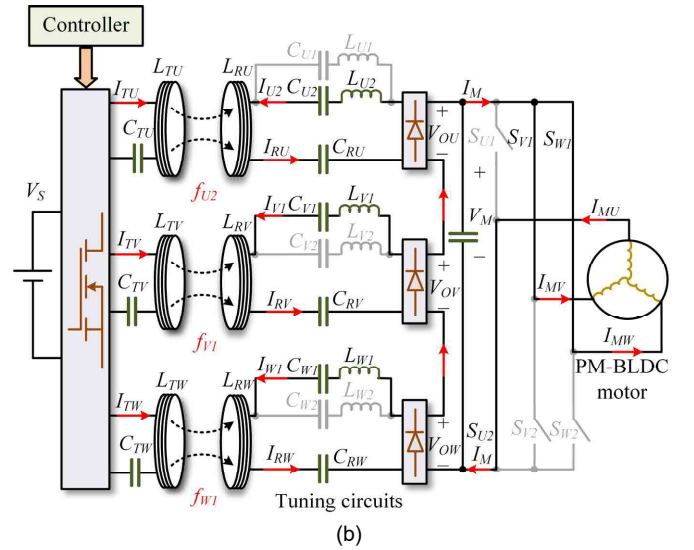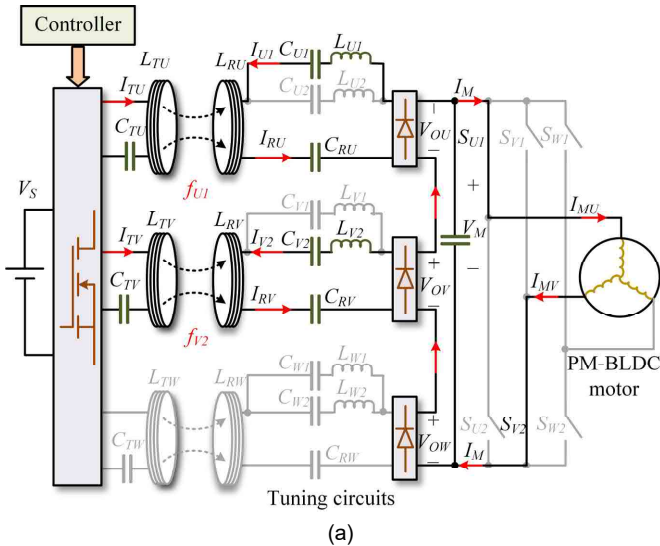

(a)

(b)

Fig. 3. Equivalent circuit of wireless PM-BLDC motor system. (a) The first sector in 120° commutation. (b) The fifth sector in 180° commutation.
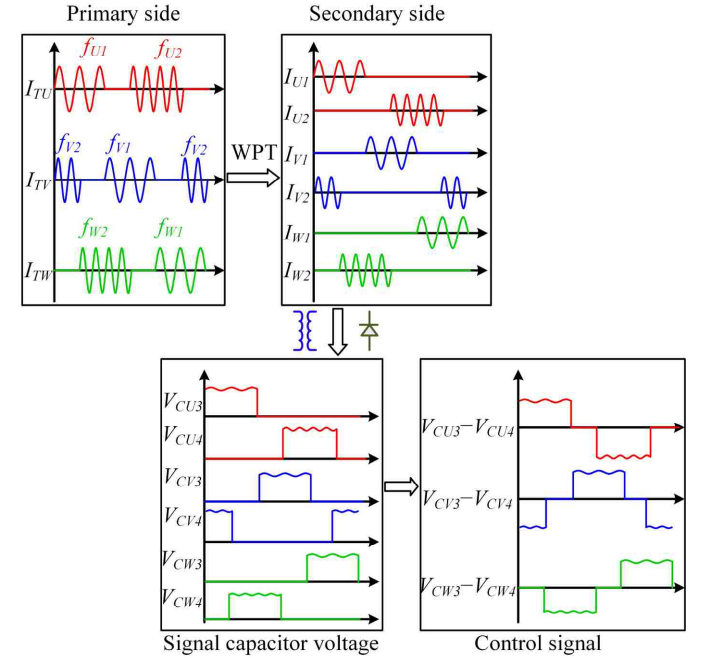

Fig. 4. 120° commutation control signal extraction flow chart.

C. Motor Voltage Control

For motor speed regulation, the motor terminal voltage is controlled at the primary side. In detail, voltages induced by the three-phase receivers V_{RU}, V_{RV}, and V_{RW} can be expressed as [28]

$$\begin{cases} V_{RU} = 2\pi f_{Ui} M_U I_{TU} \\ V_{RV} = 2\pi f_{Vi} M_V I_{TV} \qquad (i=1,2) \cdot \\ V_{RW} = 2\pi f_{Wi} M_W I_{TW} \end{cases} \qquad (3)$$

Meanwhile, the secondary rectifier output voltage V_{Oi} ($i=U$, V, W) is basically the same as the voltage induced by the receiver V_{Ri} ($i=U$, V, W), as it can be expressed as [29]

$$V_{Oi} = V_{Ri} \frac{Z_L}{Z_{Ri} + Z_{LCi} + Z_L} \qquad (i = U, V, W) \qquad (4)$$

where Z_L is the load impedance, Z_{Ri} ($i=U$, V, W) is the impedance of the receiving LC tank, and Z_{LCi} ($i=U$, V, W) is the impedance of the paralleled LC branches. To be more specific, Z_{Ri} ($i=U$, V, W) can be expressed as

$$Z_{Ri} = 2\pi f_i L_{Ri} + \frac{1}{2\pi f_i C_{Ri}} \qquad (i = U, V, W) \qquad (5)$$

where f_i ($i=U$, V, W) is the operating frequency of WPT.

By minimizing the difference between f_{i1} and f_{i2} ($i=U$, V, W), the receiving LC tank is near resonance at f_{i1} and f_{i2} ($i=U$, V, W), thus the impedance Z_{Ri} ($i=U$, V, W) can be very small at these two frequencies.

Also, in (4), Z_{LCi} ($i=U$, V, W) can be expressed as

$$Z_{LCi} = \left(2\pi f_i L_{i1} + \frac{1}{2\pi f_i C_{i1}} \right) \| \left(2\pi f_i L_{i2} + \frac{1}{2\pi f_i C_{i2}} \right) \quad (i = U, V, W) \quad (6)$$

As aforementioned, the first LC branch is resonant at the first frequency, while the second LC branch is resonant at the second frequency. Thus, when the system is operating at the first or the second frequency, (6) can be simplified as

$$Z_{LCi} = 0 \| \left(2\pi f_{i2} L_{i2} + \frac{1}{2\pi f_{i2} C_{i2}} \right) = 0 \qquad (i = U, V, W) \qquad (7)$$

or

$$Z_{LCi} = \left(2\pi f_{i1} L_{i1} + \frac{1}{2\pi f_{i1} C_{i1}} \right) \| 0 = 0 \qquad (i = U, V, W) \qquad (8)$$

respectively.

Therefore, (4) can be simplified as

$$V_{Oi} = V_{Ri} \frac{Z_L}{Z_{Ri} + Z_{LCi} + Z_L} \approx V_{Ri} \qquad (i = U, V, W) \qquad (9)$$

which means the rectifier output voltage is basically the same as the receiver-induced voltage. Thus, the voltage of the DC-link at the secondary side V_M can be expressed as

$$V_M = \sum V_{Oi} \approx \sum V_{Ri} = 2\pi \sum f_i M_i I_{Ti} \qquad (i = U, V, W) \qquad (10)$$

Therefore, both the phase sequences and phase voltages at the motor terminals can be controlled from the primary side.
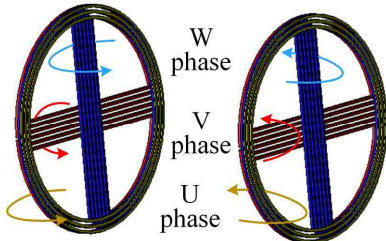

Fig. 5. Orthogonal structure of three-phase WPT coils.

III. SYSTEM DESIGN

A. Placement of Three-Phase WPT Coils

In order to securely feed the three-phase stator windings, three pairs of WPT coils are employed. Since the mutual inductance between coils will affect WPT to individual phases and thus deteriorate the selectivity among phases, the three pairs of WPT coils should be arranged with sufficient clearance so as to suppress the mutual inductance [23]. However, this will make the system bulky and difficult to be packed.

Alternatively, considering the frequencies for three-phase power transmission can be set differently with each other, the three-phase WPT coils can overlap each other, and only the resonant receiver circuit can acquire the energy from the transmitter. However, the system selectivity highly depends on the frequency gap between the different phases. If the frequency gap is too small, the selectivity is insufficient; if the frequency gap is too large, the transmission performances of different phases will be different, thus it will be difficult to balance the transmission power between different phases.

Consequently, an orthogonal structure [30] is adopted, which is very compact as it contains two bipolar coils and one unipolar coil, as shown in Fig. 5. Since the magnetic circuits of different phases do not coincide, the mutual inductances between different phases are theoretically zero [31].

B. Compensation Circuit and WPT Frequency Selection

As mentioned above, each of the three phases of the system uses two frequencies.

In order to simplify the transmitting and receiving circuits, only one capacitor is employed as the resonant compensation. Thus, to ensure near-resonant operation, the difference between the two frequencies of the same phase should be small, i.e., less than 10 kHz. Also, the inductances of the WPT coils L_{Ti} and L_{Ri} ($i=U$, V, W) should be smaller to reduce the impedance Z_{Ri} ($i=U$, V, W) in (5). Thus, about 30 mH coils are finally employed for the WPT.

However, mutual inductances will be limited with such small L_{Ti} and L_{Ri} ($i=U$, V, W), which will impair the connection between the primary and secondary sides, as the voltages induced by receivers may be insufficient, according to (3). Also, the system's efficiency may be sacrificed, as the equivalent impedance of the secondary side Z'_{2i} ($i=U$, V, W) is very small at the primary side, which can be expressed as [32]

$$\begin{cases} Z'_{2U} = \dfrac{(2\pi f_{Ui} M_U)^2}{Z_{2U}} \\[2mm] Z'_{2V} = \dfrac{(2\pi f_{Vi} M_V)^2}{Z_{2U}} \qquad (i = 1, 2) \\[2mm] Z'_{2W} = \dfrac{(2\pi f_{Wi} M_W)^2}{Z_{2W}} \end{cases} \qquad (11)$$

Thus, the energy lost at the transmitting circuit's inner resistance R_{1i} ($i=U$, V, W) will have a higher ratio, as R_{1i} and Z'_{2i} ($i=U$, V, W) are series-connected. To solve these problems, the frequency should be higher, according to (3) and (11).

Meanwhile, the operating frequency cannot be infinitely high. Otherwise, it will cause higher eddy current loss, tissue heating of surrounding people, and more switching loss [22]. Therefore, taking into account these trade-offs, we finally selected the operating frequency of around 350 kHz.

C. LC Tuning Circuit Design

As LC tuning circuits are employed to supply control signals, the accuracy of inductance and capacitance is very important. Thus, inductors with iron cores appear not appropriate. Otherwise, the inductances, as well as the resonant frequency, would drift with different receiver currents because of B–H (flux density-magnetic field strength) nonlinearities.

Meanwhile, to provide sufficient voltages of control signals, i.e., 10 V for most MOSFETs, the capacitances should be very low. Taking the U-phase as an example, the control signal can be calculated from [18]

$$V_{CU3} - V_{CU4} = |V_{CU1}| - |V_{CU2}|$$
$$= \frac{|I_{U1}|}{j2\pi f_{Ui}C_{U1}} - \frac{|I_{U2}|}{j2\pi f_{Ui}C_{U2}} \quad (i = 1, 2) \quad (12)$$

where I_{U1} and I_{U2} can be expressed as

$$\begin{cases} I_{U1} = I_U \dfrac{Z_{U2}}{(Z_{U1} + Z_{U2})} \\ I_{U2} = I_U \dfrac{Z_{U1}}{(Z_{U1} + Z_{U2})} \end{cases} . \quad (13)$$

Hence, (12) can be rewritten as

$$V_{CU3} - V_{CU4} = |I_U| \frac{1}{j2\pi f_{Ui}(Z_{U1} + Z_{U2})} \left(\frac{Z_{U2}}{C_{U1}} - \frac{Z_{U1}}{C_{U2}} \right) \quad (i = 1, 2). \quad (14)$$

Further, when the system is operating at f_{U1}, the first LC tuning circuit is in fully resonant condition, and (14) can be simplified as

$$V_{CU3} - V_{CU4} = |I_U| \frac{1}{j2\pi f_{U1}C_{U1}} . \quad (15)$$

Similarly, when the system is operating at f_{U2}, (14) can be simplified as

$$V_{CU3} - V_{CU4} = |I_U| \frac{-1}{j2\pi f_{U2}C_{U2}} . \quad (16)$$

Meanwhile, considering three phases are employed to charge the motor at the same time in the 180° commutation method, I_U is basically one-third of the motor current. Thus, with the given minimum motor current in no-load condition, the largest capacitances of the LC tuning circuits can be derived, following

$$\begin{cases} C_{U1} \leq \dfrac{|I_M|}{3} \dfrac{1}{j2\pi f_{U1}|V_{CU3} - V_{CU4}|} \approx \dfrac{|I_M|}{j6\pi f_{U1} \times 10} \\ C_{U2} \leq \dfrac{|I_M|}{3} \dfrac{1}{j2\pi f_{U2}|V_{CU3} - V_{CU4}|} \approx \dfrac{|I_M|}{j6\pi f_{U2} \times 10} \end{cases} . \quad (17)$$

D. Secondary Inverter Design

For three-phase wireless power transmission, multi kinds of topology can be selected. For example, the system can employ one or two pairs of WPT coils to charge the PM-BLDC motor, as shown in Fig. 6. Furthermore, wireless switches were proposed for the secondary controller-less inverter [13], as

shown in Fig. 7. However, these topologies are not suitable for a wireless PM-BLDC, the main reason is that the power transmitter and receiver need three-frequency or six-frequency compensation, which generally results in a high-order network and is rather difficult to achieve.

As an alternative, there are two possible connections of the three-phase rectifier bridges: one refers to a parallel connection of the rectifier bridges, while another is the series connection, as shown in Fig.8(a) and (b).

For the series structure, the motor current will flow through each rectifier bridge so that the diode voltage drops and conduction losses accumulate three times the former one. However, a parallel connection of the output of rectifier bridges, which are the DC power sources at the secondary side, may become unstable. The main problem is that the ideal current sharing between the various rectifier bridges cannot be assured [33]. In real-world applications, because of unbalanced WPT, the voltages induced by different receivers should be different. Thus, the low-voltage rectifier bridge cannot output power at the parallel connection circuit [34]. Hence, the current of the LC tuning circuit and the voltage of the corresponding capacitor will be insufficient to switch on the MOSFET.

Therefore, the three-phase rectifier bridges are series connected at the secondary side. To reduce the power loss of the series connected rectifier bridges, a low-voltage-drop diode is parallel connected to each rectifier bridge.
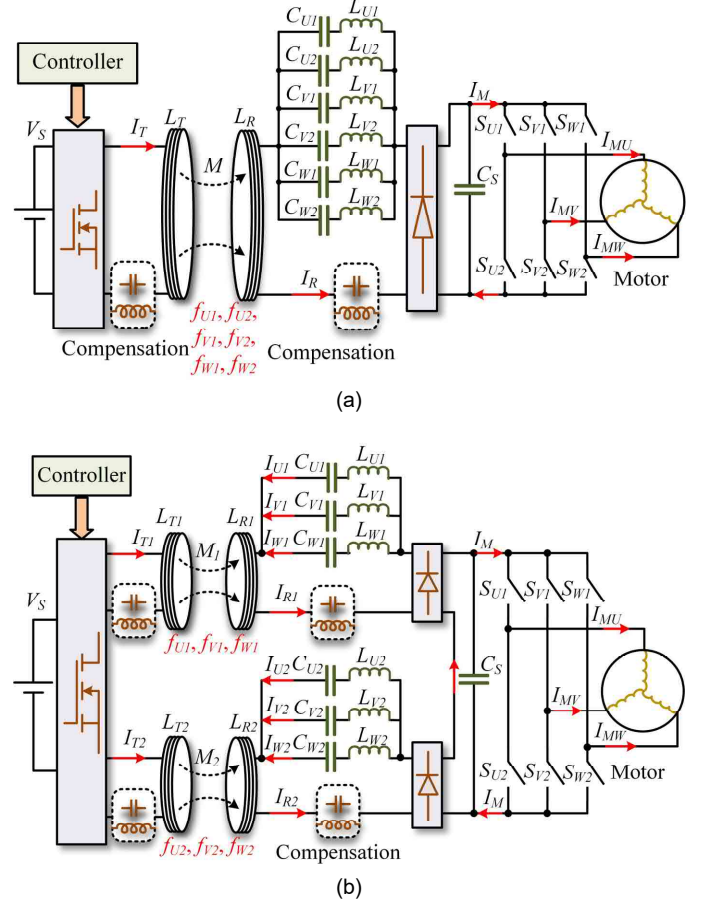

(a)

(b)

Fig. 6. Secondary controller-less wireless PM-BLDC with fewer WPT coils. (a) With one pair of WPT coils. (b) With two pairs of WPT coils.
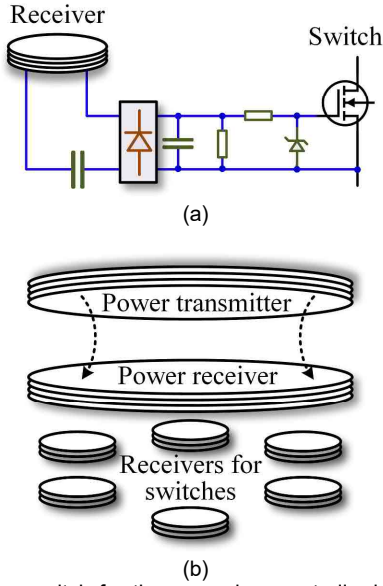

(a)

(b)

Fig. 7. Wireless switch for the secondary controller-less inverter. (a) Circuit of the wireless switch. (b) Placement of WPT coils and signal receivers.
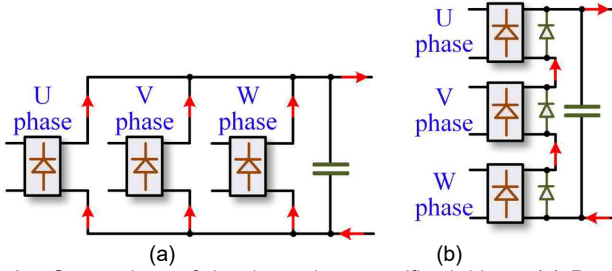

(a)   (b)

Fig. 8. Connections of the three-phase rectifier bridges. (a) Parallel connection. (b) Series connection.

TABLE II
SYSTEM PARAMETERS

| Item	Value/Type	Unit
WPT frequencies ($f_{U1}, f_{U2}, f_{V1}, f_{V2}, f_{W1}, f_{W2}$)	299, 305, 324, 332, 350, 359	kHz
Transmitter coil inductances (L_{TU}, L_{TV}, L_{TW})	26, 33.5, 33.5	µH
Receiver coil inductances (L_{RU}, L_{RV}, L_{RW})	26, 33.5, 33.5	µH
Mutual inductances (M_U, M_V, M_W)	8.3, 8.5, 8.5	µH
Transmitter compensation capacitances (C_{TU}, C_{TV}, C_{TW})	10.6, 7, 6	nF
Receiver compensation capacitances (C_{RU}, C_{RV}, C_{RW})	10.6, 7, 6	nF
Diameter of WPT coils	19	cm
LC tuning circuit inductances ($L_{U1}, L_{U2}, L_{V1}, L_{V2}, L_{W1}, L_{W2}$)	28.3, 27.2, 24, 23, 23, 21.8	µH
LC tuning circuit capacitances ($C_{U1}, C_{U2}, C_{V1}, C_{V2}, C_{W1}, C_{W2}$)	10, 10, 10, 10, 9, 9	nF
Signal transformer	ILR-11-0003	
The model of Zener	1N4741	
N-channel MOSFET	C3M0065090	
P-channel MOSFET	IXTX32P60P	
Model of PM-BLDC motor	QBL5704-94-04-032	
Rated speed of PM-BLDC motor	4000	rpm
Rated input power of PM-BLDC motor	134	W
Rated input voltage of PM-BLDC motor	36	V

(a)

(b)
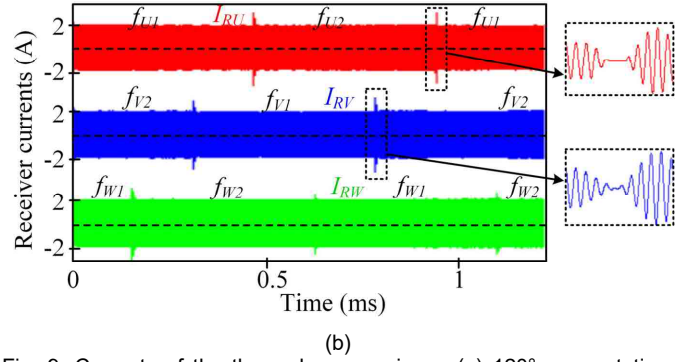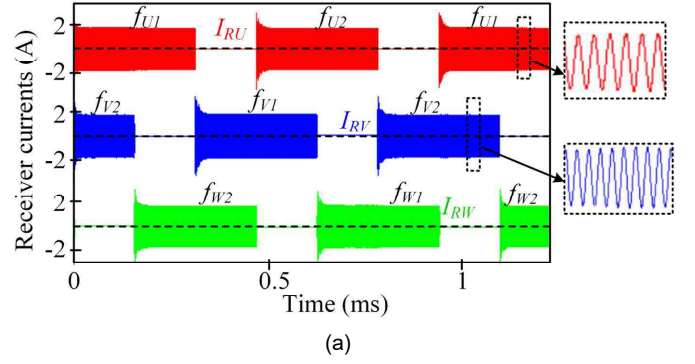
Fig. 9. Currents of the three-phase receivers. (a) 120° commutation. (b) 180° commutation.

IV. CONTROL PERFORMANCE ANALYSIS

A circuit simulation with the key parameters listed in Table II demonstrates and analyzes the performance of the proposed wireless PM-BLDC motor system. Three star-connected 20 Ω resistors represent the three-phase PM-BLDC motor as an approximation.

When charging three-phase transmitters in the designed sequence, three-phase receivers can harvest wireless energy, accordingly, as shown in Fig. 9.

Also, as discussed above, the primary side can selectively switch on or off the secondary MOSFET by regulating the WPT frequency to resonate the corresponding LC tuning circuit, and the currents are given in Fig. 10. Hence, the control voltages for the secondary three-phase inverter can be acquired, as shown in Fig. 11. Therefore, the three-phase AC power for the load can be achieved at the secondary side, as shown in Fig. 12.
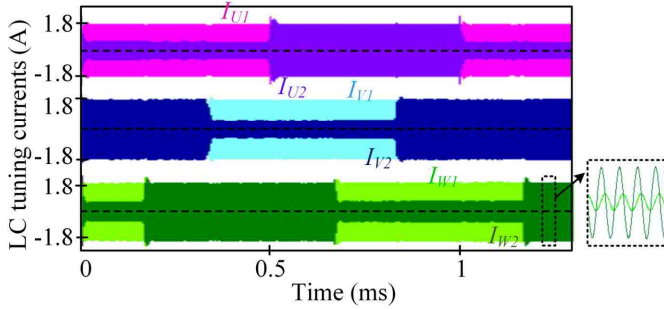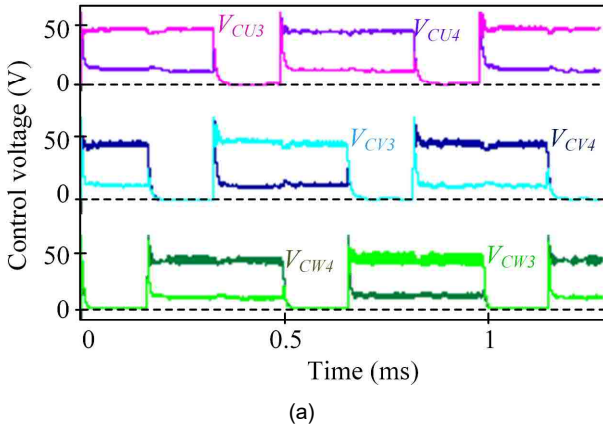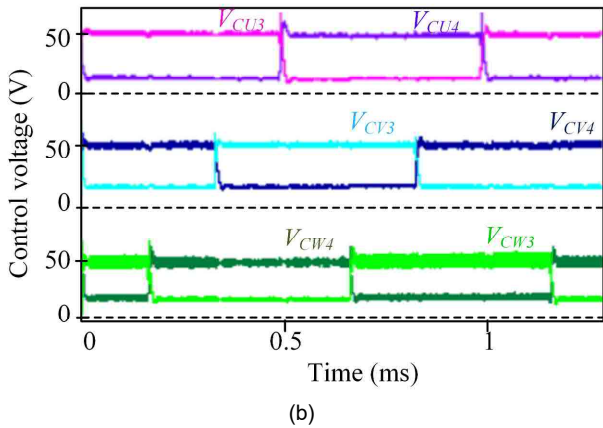

(a)

(b)
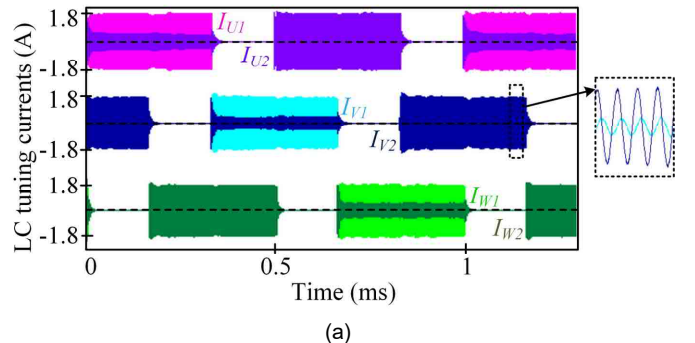
Fig. 10. Currents of six LC tuning circuits. (a) 120° commutation. (b) 180° commutation.
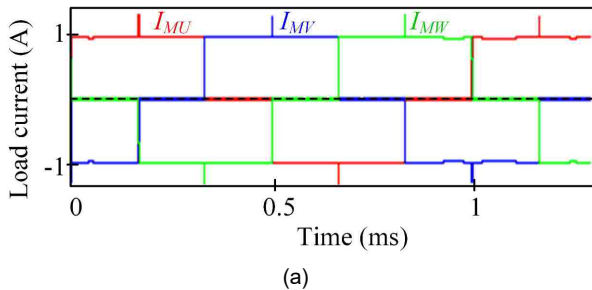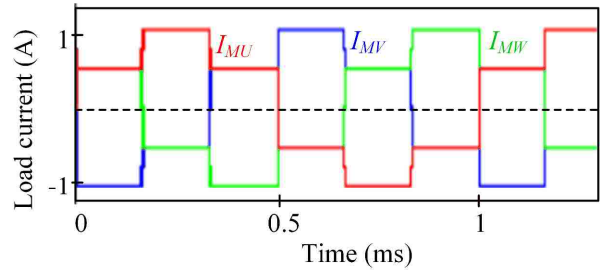

(a)

(b)

Fig. 11. The rectified voltages of six capacitors in LC tuning circuits. (a) 120° commutation. (b) 180° commutation.
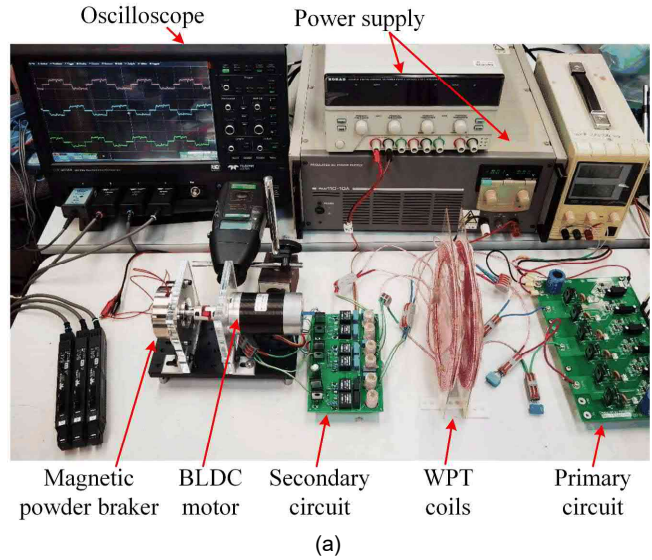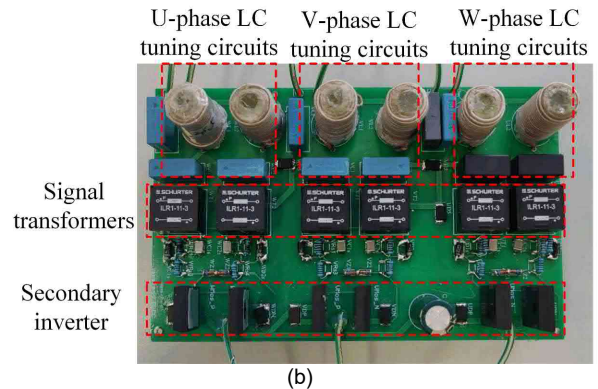

(a)

(b)

Fig. 12. Three-phase AC currents for PM-BLDC motor. (a) 120° commutation. (b) 180° commutation.

(a)

(b)

Fig. 13. Implementation of wireless PM-BLDC motor. (a) Experimental prototype. (b) Secondary controller-less circuit.

V. IMPLEMENTATION AND EXPERIMENTAL RESULTS

To verify the feasibility of the proposed wireless PM-BLDC motor system, we implemented a prototype, as shown in Fig. 13. The model of the load PM-BLDC motor is QBL5704-94-04-032 with a rated voltage of 36 V, a rated power of 134 W, and a maximum speed of 4000 rpm. As 180° commutation is already proved in simulation, only the 120° commutation operation is verified in this experiment.

When the primary side provides three-phase wireless power with a 3.75 ms period, as shown in Fig. 14, receivers receive these energies and charge the load motor. Meanwhile, six LC

tuning circuits resonate at the corresponding frequency, and capacitors in LC tuning circuits are charged alternatively, as shown in Fig. 15. Hence, after rectifying and stabilizing, the control signal can be acquired, as shown in Fig. 16 (a) and (b). As a result, the PM-BLDC motor can be self-driven and rotate at 4000 rpm, as shown in Fig. 17.
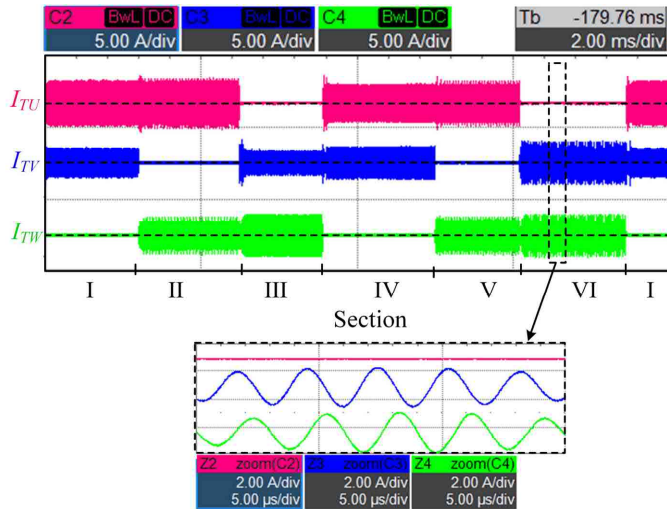

Fig. 14. Currents of three-phase transmitters.
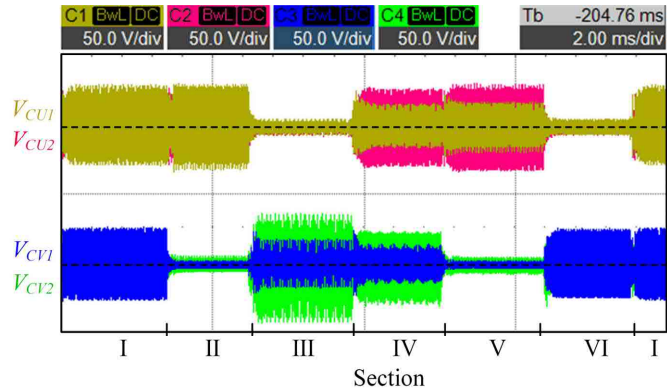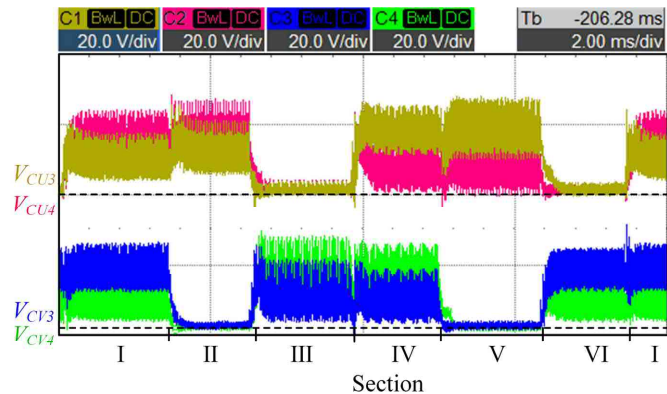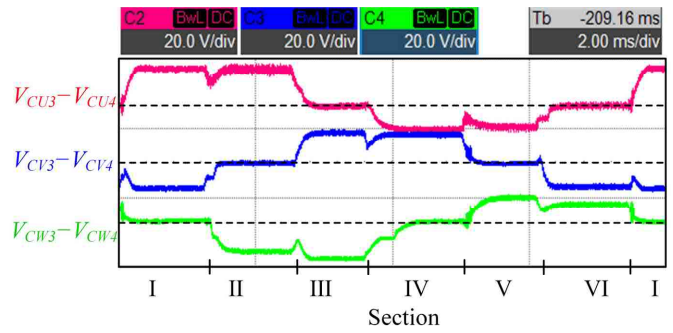

Fig. 15. Currents of U-phase and V-phase LC tuning circuits.

(a)

(b)

Fig. 16. Control voltages of the secondary converter. (a) Capacitor voltages at U-phase and V-phase LC tuning circuits. (b) Voltage difference of rectified and filtered capacitor voltages of LC tuning circuits.
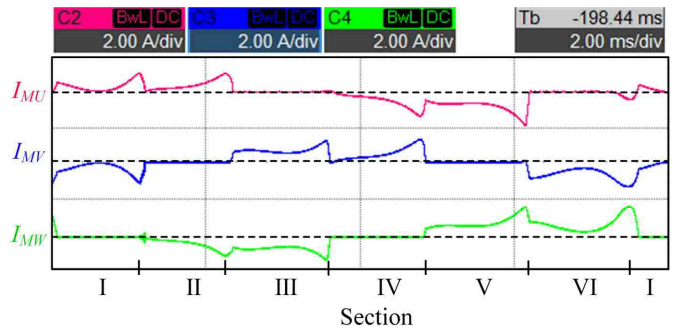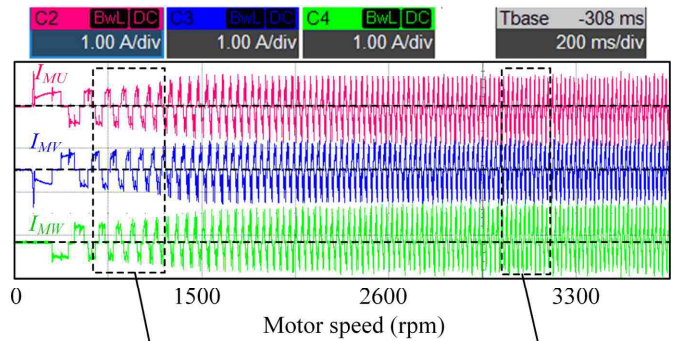

Fig. 17. Motor currents at 4000 rpm.

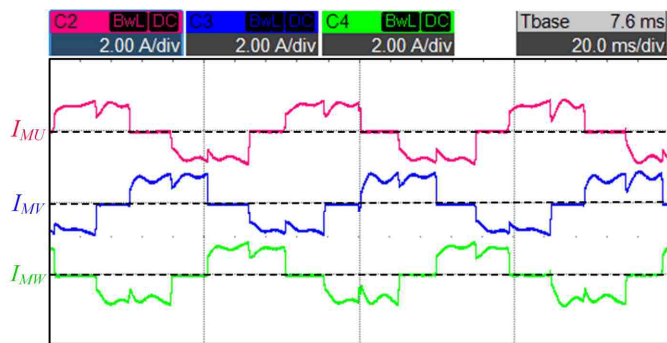Fig. 18. Motor currents during acceleration.

Fig. 19. Motor currents at 1000 rpm with 10 N·cm load.

Moreover, this system has a faster response speed. As shown in Fig. 18, the PM-BLDC motor can speed up from the idle state to 3000 rpm within 1 second,

Besides, the system also can work well under load. When charging the magnetic carbon braker to increase the motor load from 0 to 10 N·cm, the motor current increases to 0.4 A, as shown in Fig. 19.

Although the primary and secondary sides are not operating at full resonance, the WPT efficiency still can reach 93% with a 20 mm wireless transfer distance. It should be mentioned that the efficiency is positively related to the operating frequency, which is consistent with the theory analysis in Section III. Moreover, with the given parameters in Table II, the efficiency from the primary DC power source to the motor terminal is 80.2%, as the secondary rectifier bridge and inverter cause additional losses.

VI. Conclusion

This paper proposes and analyzes a secondary controller-less wireless PM-BLDC. The key is to control the secondary inverter through a self-drive circuit. By eliminating the fragile microchip, this system has the definite advantage of being robust, rendering it attractive for working in isolated environments, such as robotic arms or piping networks. Moreover, the PM-BLDC motor does not need to follow a special design; instead, most three-phase PM-BLDC motors are compatible. Circuit models and an experimental prototype validate the concept. These confirm that this system operates well for a three-phase PM-BLDC motor from 400 rpm to 4000 rpm with 20 mm WPT distance. For future research, sensorless control methods and secondary-inverter-less circuits for wireless motors will be studied: For rotor position, although wireless resolvers for rotor position measurement are robust and can provide timely position signals, they increase the cost; for secondary-inverter-less circuits, the so-called envelope circuit may be a promising technology [35]. Although the efficiency is only about 10% now, it can decouple the wireless power to provide low-frequency AC power to drive the load motor. As long as system efficiency can be improved, the PMSM can be wirelessly driven and work in isolated environments.

References

[1] J. Perzow, "Ranking Qi wireless power transmitters by efficiency," *IEEE Power Electron. Mag.*, vol. 9, no. 3, pp. 56-64, Sept. 2022.

[2] H. Feng, R. Tavakoli, O. C. Onar, and Z. Pantic, "Advances in high-power wireless charging systems: Overview and design considerations," *IEEE Trans. Transp. Electrification,* vol. 6, no. 3, pp. 886-919, Sept. 2020.

[3] P. K. Chittoor, B. Chokkalingam, and L. Mihet-Popa, "A review on UAV wireless charging: Fundamentals, applications, charging techniques and standards," *IEEE Access,* vol. 9, pp. 69235-69266, 2021.

[4] J. C. Chen, P. Kan, Z. Yu, et. al., "A wireless millimetric magnetoelectric implant for the endovascular stimulation of peripheral nerves," *Nat. Biomed. Eng,* vol. 6, no. 6, pp. 706-716, Mar. 2022.

[5] M. Song, P. Jayathurathnage, E. Zanganeh, et. al., "Wireless power transfer based on novel physical concepts," *Nat. Electron.*, vol. 4, no. 10, pp. 707-716, Oct. 2021.

[6] A. Abdolkhani, A. P. Hu, and N. K. C. Nair, "A double stator through-hole type contactless slipring for rotary wireless power transfer applications," *IEEE Trans. Energy Convers.*, vol. 29, no. 2, pp. 426-434, Jun 2014.

[7] C. Jiang, K. T. Chau, Y. Y. Leung, C. Liu, C. H. T. Lee, and W. Han, "Design and analysis of wireless ballastless fluorescent lighting," *IEEE Trans. Ind. Electron.*, vol. 66, no. 5, pp. 4065-4074, May 2019.

[8] H. Sarnago, O. Lucia, and J. M. Burdio, "A versatile resonant tank identification methodology for induction heating systems," *IEEE Trans. Power Electron.*, vol. 33, no. 3, pp. 1897-1901, Mar. 2018.

[9] M. Vandeputte, L. Dupre, and G. Crevecoeur, "Quasi-static torque profile expressions for magnetic resonance-based remote actuation," *IEEE Trans. Energy Convers.*, vol. 34, no. 3, pp. 1255-1263, Sep. 2019.

[10] C. H. Li, Z. Wang, and Y. Xu, "A wireless-power-transfer-based three-phase PMSM drive system with matrix converter," *IEEE Trans. Ind. Electron.*, vol. 70, no. 3, pp. 2307-2317, Mar. 2023.

[11] A. Kawamura, K. Ishioka, and J. Hirai, "Wireless transmission of power and information through one high-frequency resonant AC link inverter for robot manipulator applications," *IEEE Trans. Ind. Appl.*, vol. 32, no. 3, pp. 503-508, May-Jun. 1996.

[12] W. Liu, K. T. Chau, H. Wang, and T. Yang, "Long-range wireless power drive using magnetic extender," *IEEE Trans. Transp. Electrification,* vol. 9, no. 1, pp. 1897-1909, Mar. 2023.

[13] W. Liu, K. T. Chau, C. H. T. Lee, L. B. Cao, and W. Han, "Wireless power and drive transfer for piping network," *IEEE Trans. Ind. Electron.*, vol. 69, no. 3, pp. 2345-2356, Mar. 2022.

[14] J. H. Kim, B. S. Lee, J. H. Lee, et. al., "Development of 1-MW inductive power transfer system for a high-speed train," *IEEE Trans. Ind. Electron.*, vol. 62, no. 10, pp. 6242-6250, Oct. 2015.

[15] M. Sato, G. Yamamoto, D. Gunji, T. Imura, and H. Fujimoto, "Development of wireless in-wheel motor using magnetic resonance coupling," *IEEE Trans. Power Electron.*, vol. 31, no. 7, pp. 5270-5278, Jul. 2016.

[16] T. Tan, K. N. Chen, Y. Jiang, Q. Q. Lin, L. Q. Yuan, and Z. M. Zhao, "A bidirectional wireless power transfer system control strategy independent of real-time wireless communication," *IEEE Trans. Ind. Appl.*, vol. 56, no. 2, pp. 1587-1598, Mar.-Apr. 2020.

[17] C. Jiang, K. T. Chau, C. Liu, and W. Han, "Wireless DC motor drives with selectability and controllability," *Energies*, vol. 10, no. 1, Jan. 2017.

[18] H. Wang, K. T. Chau, C. H. T. Lee, L. Cao, and W. H. Lam, "Design, analysis, and implementation of wireless shaded-pole induction motors," *IEEE Trans. Ind. Electron.*, vol. 68, no. 8, pp. 6493-6503, Jul. 2021.

[19] C. Jiang, K. T. Chau, W. Liu, C. Liu, W. Han, and W. H. Lam, "An LCC-compensated multiple-frequency wireless motor system," *IEEE Trans. Industr. Inform.*, vol. 15, no. 11, pp. 6023-6034, Nov. 2019.

[20] H. Wang, W. Liu, and K. T. Chau, "Wireless motors – a new breed of power electronics drives," *2022 IEEE 9th ICoPESA*, Hong Kong, Sept. 2022.

[21] H. S. Seol, J. Lim, D. W. Kang, J. S. Park, and J. Lee, "Optimal design strategy for improved operation of IPM BLDC motors with low-resolution hall sensors," *IEEE Trans. Ind. Electron.*, vol. 64, no. 12, pp. 9758-9766, Dec. 2017.

[22] S. Cho, J. Hwang, and C.-W. Kim, "A study on vibration characteristics of brushless DC motor by electromagnetic-structural coupled analysis using entire finite element model," *IEEE Trans. Energy Convers.*, vol. 33, no. 4, pp. 1712-1718, Dec. 2018.

[23] C. Jiang, K. T. Chau, C. Liu, and W. Han, "Design and analysis of wireless switched reluctance motor drives," *IEEE Trans. Ind. Electron.*,

vol. 66, no. 1, pp. 245-254, Jan. 2019.

[24] C. Y. Xia, R. H. Jia, Y. T. Shi, A. P. Hu, and Y. Zhou, "Simultaneous wireless power and information transfer based on phase-shift modulation in ICPT system," *IEEE Trans. Energy Convers.,* vol. 36, no. 2, pp. 629-639, Jun. 2021.

[25] H. Wang, K. T. Chau, C. H. T. Lee, and X. Tian, "Design and analysis of wireless resolver for wireless switched reluctance motors," *IEEE Trans. Ind. Electron.,* vol. 70, no. 3, pp. 2221-2230, Mar. 2023.

[26] A. S. Al-Adsani, M. E. AlSharidah, and O. Beik, "BLDC motor drives: A single hall sensor method and a 160 degrees commutation strategy," *IEEE Trans. Energy Convers.,* vol. 36, no. 3, pp. 2025-2035, Sep. 2021.

[27] A. Sen and B. Singh, "Gradient detection starting controlled photovoltaic sourced BLDCM drive without position sensors," *IEEE Trans. Energy Convers.,* vol. 37, no. 3, pp. 1611-1622, Sep. 2022.

[28] M. Liu, K. W. Chan, J. F. Hu, Q. F. Lin, J. W. Liu, and W. Z. Xu, "Design and realization of a coreless and magnetless electric motor using magnetic resonant coupling technology," *IEEE Trans. Energy Convers.,* vol. 34, no. 3, pp. 1200-1212, Sept. 2019.

[29] A. Babaki, S. Vaez-Zadeh, A. Zakerian, and A. Jafari Natanzi, "Analysis and control of wireless motor drives with a single inverter in primary side," *IEEE Trans. Energy Convers.,* vol. 36, no. 2, pp. 930-939, Jun. 2021.

[30] X. Zhang, Y. M. Zhang, Z. M. Zhang, and M. Y. Li, "Mode conversion and structure optimization of quadrature coils for electric vehicles wireless power transfer," *IEEE Trans. Energy Convers.,* vol. 35, no. 2, pp. 575-590, Jun. 2020.

[31] A. Zaheer, H. Hao, G. A. Covic, and D. Kacprzak, "Investigation of multiple decoupled coil primary pad topologies in lumped IPT systems for interoperable electric vehicle charging," *IEEE Trans. Power Electron.,* vol. 30, no. 4, pp. 1937-1955, Apr. 2015.

[32] A. Babaki, S. Vaez-Zadeh, A. Zakerian, and G. A. Covic, "Variable-frequency retuned WPT system for power transfer and efficiency improvement in dynamic EV charging with fixed voltage characteristic," *IEEE Trans. Energy Convers.,* vol. 36, no. 3, pp. 2141-2151, Sept. 2021.

[33] S. J. Wang, K. Gao, Y. F. Ge, et. al., "Discussion on the relationship between ups battery connection method and its reliability," *2018 Ninth International Conference on Intelligent Control and Information Processing (ICICIP)*, Wanzhou, China, pp. 144-147, 2018.

[34] M. Y. Guan, "A series-connected offshore wind farm based on modular dual-active-bridge (DAB) isolated DC-DC converter," *IEEE Trans. Energy Convers.,* vol. 34, no. 3, pp. 1422-1431, Sep. 2019.

[35] Hiroaki Ota, Jia Liu, Yushi Miura, et. al., "Multiphase direct AC wireless power transfer system: Comparative proposals using frequency and amplitude modulations," *IEEE Trans. Emerg. Sel. Topics Power Electron.,* vol. 2, no. 2, pp. 101-112, Apr. 2021.

K. T. Chau (M'89–SM'04–F'13) received the B.Sc. (Eng.), M.Phil., and Ph.D. degrees in electrical and electronic engineering from The University of Hong Kong (HKU), Hong Kong, in 1988, 1991, and 1993, respectively. He worked at HKU for 28 years, with various positions including the Director of International Research Centre for Electric Vehicles, Associate Dean of Engineering and Head of Department of Electrical and Electronic Engineering. Starting from 2023, he serves as Chair Professor of Electrical Energy Engineering at the Department of Electrical and Electronic Engineering in the Hong Kong Polytechnic University (PolyU). His research interests include electric and hybrid vehicles, power electronics and drives, and renewable energies in which he has published nine books and more than 350 journal papers.

Prof. Chau is a Fellow of the Institution of Engineering and Technology (IET), U.K., and Hong Kong Institution of Engineers (HKIE). He is currently the Co-Editor of the Journal of Asian Electric Vehicles. He is a Chartered Engineer in Hong Kong. He was the recipient of the Changjiang Chair Professorship from the Ministry of Education, China, and the Environmental Excellence in Transportation Award for Education, Training, and Public Awareness from the Society of Automotive Engineers (SAE) International.

Wei Liu (S'17–M'21) received the B.Eng. and M.Eng. degrees in electrical engineering from China University of Petroleum, Qingdao, China, and the Ph.D. degree in electrical and electronic engineering from The University of Hong Kong (HKU), Hong Kong, China, in 2014, 2017, and 2021, respectively.

He is currently a Research Assistant Professor with the Department of Electrical and Electronic Engineering, HKU, where he previously served as a Postdoctoral Fellow. He also worked as a Visiting Researcher with Nanyang Technological University, Singapore (NTU), since 2019. His research interests include wireless power transfer, power electronics and artificial intelligence, biomedical power electronics, and electric vehicle technologies.

Dr. Liu was the recipient of Power Engineering Prize from HKU, Excellent Paper Awards and Best Presentation Award from international conferences in the area of Electric Vehicles and Transportation Electrification. He is also a Guest Associate Editor of IEEE Journal of Emerging and Selected Topics in Power Electronics (JESTPE), Guest Editor of international journals, and Session Chair of international conferences.

Hui Wang (S'18–M'22) received the B.Eng. degree in electrical and electronic engineering from Shandong University of Science and Technology, Qingdao, China, in 2014, and the M.Eng. degree in electrical and electronic engineering from Tianjin University, Tianjin, China, in 2017. In 2022, he received the Ph.D. degree in electrical and electronic engineering in the University of Hong Kong, Pokfulam, Hong Kong, China.

He is currently a Postdoctoral Fellow with the Department of Electrical and Computer Engineering, Duke University, USA. Before that, he worked as a Postdoctoral Fellow with the Department of Electrical and Electronic Engineering, HKU. His research interests include electric machines and wireless power transfer technologies.

Stefan M. Goetz (Member, IEEE) received the Undergraduate and Graduate degrees from TU Muenchen, Munich, Germany, and the Ph.D. degree from TU Muenchen and from Columbia University, New York, NY, USA, in 2012 (with a thesis on medical applications of power electronics for which he was awarded a Ph.D. thesis prize from TU Muenchen).

His research interests include modular power electronics in general, precise high-power pulse synthesizers for magnetic neurostimulation, as well as integrative power electronics solutions for microgrids and electric vehicle applications.